International Journal of General Medicine

Dovepress
Taylor & Francis Group

Open Access Full Text Article

ORIGINAL RESEARCH

Metalloproteinase-9 as a Pyroptosis-Hypoxia Synergy Effector Drives Immune Remodeling in Ischemic Stroke: A Multi-Omics Validated Diagnostic Biomarker and Therapeutic Target

Jun Wu*, Da Wu*, Ming Qi, Kuan Jiang

Department of Neurosurgery, Yixing People's Hospital, Yixing, Jiangsu, People's Republic of China

*These authors contributed equally to this work

Correspondence: Kuan Jiang, Department of Neurosurgery, Yixing People's Hospital, Yixing, Jiangsu, People's Republic of China, Email staff1671@yxph.com

Purpose: As a predominant contributor to disability and premature mortality worldwide, ischemic stroke (IS) urgently requires breakthroughs in early diagnostic biomarkers. The synergistic regulatory roles of pyroptosis and hypoxia, two critical pathological mechanisms in IS, require systematic exploration.

Patients and Methods: We integrated two IS peripheral blood transcriptomic datasets (GSE66724 and GSE58294) to identify differentially expressed genes (DEGs) linked to pyroptosis and hypoxia. Co-expression networks were constructed using weighted gene co-expression network analysis. Diagnostic biomarkers were identified through the Least Absolute Shrinkage and Selection Operator, Support Vector Machine, and Random Forest algorithms, with validation performed in an independent cohort (GSE16561) and real-time quantitative PCR (RT-qPCR). Single-cell sequencing (GSE174574) was used to map cellular expression patterns of diagnostic genes. Candidate drugs were identified through the Connectivity Map (CMAP) database, with molecular docking validating their target protein interactions.

Results: We identified 32 pyroptosis-related and 50 hypoxia-related DEGs, with enrichment analyses indicating their involvement in inflammatory responses, NF-κB signaling, and tumor necrosis factor pathways. Cross-algorithm validation identified matrix metalloproteinase-9 (MMP9) as a diagnostic biomarker. RT-qPCR revealed significantly elevated MMP9 levels in the peripheral blood of IS patients ($p < 0.01$). Immune microenvironment profiling showed positive correlations between MMP9 expression and macrophage/neutrophil infiltration. Single-cell sequencing confirmed predominant MMP9 expression in granulocytes. Drug prediction via CMAP and molecular docking identified Benperidol and Fluspirilene as high-affinity ligands for MMP9.

Conclusion: This study employed multi-omics analysis followed by experimental validation to provide robust and systematic evidence supporting the diagnostic value and therapeutic potential of MMP9 in IS.

Keywords: hypoxia, ischemic stroke, molecular docking, pyroptosis, single-cell

Introduction

Ischemic stroke (IS) remains a leading global health burden, accounting for >80% of stroke cases and contributing to substantial mortality and long-term disability.[1] Current diagnostic paradigms rely heavily on neuroimaging (computed tomography/magnetic resonance imaging) and clinical assessments. However, their delayed sensitivity in the hyperacute phase and insufficient for early intervention limit their applicability.[2] This highlights the urgent need for novel biomarkers based on the disease mechanisms.

The current literature has identified several classes of biomarkers for IS, each with distinct limitations. Angiogenesis-related molecules, such as Angiopoietin-2 and VEGF-A, exhibit elevated levels in IS patients, but studies are constrained

Received: 27 June 2025
Accepted: 26 October 2025
Published: 6 November 2025

by small sample sizes and unclear dynamic change mechanisms.[3] Inflammation-related molecules, like IL-6, lack specificity and have narrow detection time windows, rendering them susceptible to interference from systemic diseases.[4] Cell adhesion molecules, including sICAM-1 and PECAM-1, are linked to prognosis, yet trials of anti-adhesion therapies have failed due to immune responses, and certain genetic associations are population-specific.[5] The imaging potential of the immune-related molecule MHC-I has only been confirmed in mouse models, with its application in humans remaining uncertain.[6] Activators or inhibitors of signaling pathway molecules, such as Nrf2/HO-1 and NF-κB, pose off-target risks, and preclinical data lack translational support.[7] Collectively, these biomarkers face challenges, including translational bottlenecks, time-dependency, and inadequate therapeutic specificity,[8] which restricts their routine clinical application.

Emerging evidence highlights pyroptosis and hypoxia as key drivers of IS progression.[9] Pyroptosis is a type of programmed cell death characterized by a pro-inflammatory response, which intensifies brain injury by causing the rupture of the plasma membrane and the subsequent release of pro-inflammatory cytokines.[10,11] In the pathological process of IS, hypoxia, a core pathogenic factor, directly triggers inflammatory vesicle activation and pyroptosis via oxygen-glucose deprivation induced by disruption of cerebral blood flow.[12–14] Pyroptosis, in turn, amplifies hypoxic injury through the inflammatory cascade, creating a vicious cycle. However, current mechanistic studies are primarily based on animal models or in vitro cell lines, which exhibit significant species differences compared to human stroke.[12] While NLRP3 inflammasome activation links pyroptosis to neurovascular injury,[15] the synergistic mechanisms between pyroptotic pathways and hypoxic signaling remain poorly understood, hindering the advancement of multi-target therapeutic strategies. Systematic integration of pyroptosis-related genes and hypoxia-related genes could reveal hub biomarkers reflecting the multifaceted IS pathology.

Advances in bioinformatics and multi-omics technologies have offered unprecedented opportunities for biomarker discovery. Public repositories such as the Gene Expression Omnibus (GEO) database (http://www.ncbi.nlm.nih.gov/geo), GeneCard database (https://www.genecards.org/),[16] and Molecular Signatures Database[17] (MSigdB) (https://www.gsea-msigdb.org/gsea/index.jsp) enable large-scale mining of transcriptomic signatures, whereas machine learning algorithms enhance diagnostic reliability. However, existing IS biomarker research remains fragmented, with prior efforts often limited to single datasets, lacking cross-sectional analysis, or failing to validate findings across single-cell RNA sequencing (scRNA-seq) dataset.[18]

This study employed a comprehensive research approach to systematically tackle existing issues. Initially, differential expression analysis was performed using transcriptomic data from the GEO database, differentially expressed genes (DEGs) were intersected with pyroptosis-related genes and hypoxia-related genes, respectively. Next, weighted gene co-expression network analysis (WGCNA) was combined with machine learning algorithms (Least Absolute Shrinkage and Selection Operator [LASSO], Support Vector Machine [SVM], and Random Forest [RF]) for multimodal feature selection, pinpointing robust cross-cohort diagnostic biomarkers. The diagnostic efficacy and clinical translational value of these biomarkers were assessed using receiver operating characteristic curve (ROC) analysis. ScRNA-seq data elucidated the cell-type-specific expression patterns of the diagnostic biomarkers. Additionally, potential therapeutic compounds were screened via the Connection Mapping (CMAP) database, with molecular docking techniques evaluating their binding efficacy with target proteins. Finally, experimental validation of the diagnostic biomarkers was conducted using real-time quantitative PCR (RT-qPCR) in peripheral blood samples from patients with IS, completing a comprehensive research loop from bioinformatic prediction to experimental confirmation.

Methods

Data Collection and Processing

We queried the GEO database for "stroke", applying these criteria: 1) the species must be Homo sapiens; 2) data must be from whole-blood mRNA transcriptome microarrays; and 3) participants, both with IS and healthy controls, must be over 18 years old. This search identified three suitable datasets. The GSE66724 dataset included eight control and eight IS samples, while the GSE58294 dataset comprised 23 control and 69 IS samples, all utilizing the Affymetrix Human Genome U133 Plus 2.0 Array platform (GPL570). We extracted the control group and 23 untreated IS samples from

GSE58294, applied log2(x+1) normalization, and combined it with GSE66724 using the "sva" R package[19] to create a training set with 31 control and 31 IS samples. For validation, we analyzed the GSE16561 dataset (24 controls and 39 IS cases) using the Illumina HumanRef-8 v3.0 platform (GPL6883), imputing missing expression values with feature mean substitution. Additionally, the GSE174574 scRNA-seq dataset from brain tissue included samples from 3 sham-operated and 3 middle cerebral artery occlusion (MCAO) mice. We selected representative samples GSM5319989 (sham) and GSM5319992 (MCAO) for detailed analysis to explore cell type-specific expression patterns of diagnostic genes.

We queried the GeneCard database with the keywords "pyroptosis" and "hypoxia", applying "Protein Coding" as a filter, which yielded 624 pyroptosis-related genes and 6264 hypoxia-related genes. To refine the hypoxia-related genes, we selected only those with a relevance score above 3.0, resulting in 859 hypoxia-related genes. Additionally, we accessed MSigdB with the same keywords, retrieving the pyroptosis gene set REACTOME_PYROPTOSIS (27 genes) and the hypoxia gene set WINTER_HYPOXIA_METAGENE (243 genes). After integrating these with the GeneCard data and eliminating duplicates, we identified 624 unique pyroptosis-related genes and 970 unique hypoxia-related genes (Supplementary Table 1).

Peripheral blood samples from 12 patients with IS were collected from hospitalized individuals in the Department of Neurosurgery at Yixing People's Hospital (Supplementary Table 2). Inclusion criteria included age over 18 years, confirmed large vessel occlusion via computed tomography angiography, and sample collection within six hours of symptom onset. Control samples were sourced from 12 adult healthy volunteers at the same institution's health examination center. This study was approved by the Ethics Committee of Yixing People's Hospital (Approval No.: Lun Shen 2025 Ke 038-01). Participant recruitment occurred from March to September, 2025, and written informed consent was acquired from the family members of all participating patients.

Identification of DEGs Associated with Pyroptosis and Hypoxia

Principal component analysis (PCA) was performed to evaluate the efficacy of batch effect correction before and after dataset integration. Differential expression analysis using the "limma" R package[20] identified significantly DEGs under stringent criteria of adjusted p-value < 0.05 and |log2FC| > 0.5. DEGs were visualized through volcano plots created with the "ggplot2" R package and heatmaps constructed using the "pheatmap" R package. Intersection analysis of DEGs with pyroptosis-related genes and hypoxia-related genes identified pyroptosis-related DEGs and hypoxia-related DEGs, and their overlapping relationships were depicted using Venn diagrams.

Functional Enrichment and Pathway Analysis

To elucidate the biological mechanisms underlying pyroptosis-related DEGs and hypoxia-related DEGs, we conducted functional enrichment profiling of these genes using the "clusterProfiler" R package[21] for Gene Ontology (GO) and Kyoto Encyclopedia of Genes and Genomes (KEGG) pathway annotation. Biological terms and pathways that exhibited statistical significance ($p < 0.05$, $q < 0.1$) were subjected to rigorous selection criteria and subsequently illustrated through dot plots created with the "ggplot2" R package.

Pyroptosis and Hypoxia Signature Scores

The expression profiles of pyroptosis-related genes and hypoxia-related genes were systematically analyzed using the IS training dataset. The pyroptosis signature score along with the hypoxia signature score for each IS sample was determined employing the single-sample gene set enrichment analysis (GSEA) methodology incorporated in the "GSVA" R package.[22] Following this, the IS cohort was stratified into subgroups characterized by high and low signature scores based on median cutoff values.

WGCNA Incorporating Pyroptosis Signature Scores and Hypoxia Subgroups

To examine gene co-expression patterns in IS samples, we performed WGCNA separately for pyroptosis signature scores and hypoxia subgroups using the "WGCNA" R package.[23] The analysis workflow involved several steps. Initially, we selected the top 25% of genes with the highest expression variation (coefficient of variation) across IS samples and subjected them to normalization and outlier removal. A similarity matrix was then generated by calculating Pearson

correlation coefficients between gene pairs, which was transformed into an adjacency matrix using an optimized soft-thresholding power (β = 5). Gene co-expression relationships were assessed through topological overlap matrix computations. Subsequently, hierarchical clustering with dynamic tree cutting was applied for module identification, with parameters specifying a minimum module size of ≥50 genes and a module merging threshold set at a cut height of 0.5. Core modules were determined by examining the module eigengenes and their correlations with clinical traits (pyroptosis signature scores/hypoxia subgroups). Finally, key genes were pinpointed by overlapping pyroptosis-associated module genes with previously identified pyroptosis-related DEGs and hypoxia-associated module genes with hypoxia-related DEGs.

Diagnostic Genes Based on Multiple Machine Learning Methods

To identify diagnostic genes for IS among the key genes mentioned earlier, we developed multiple machine learning models using samples from both IS and control groups.

We employed LASSO and SVM algorithms to prioritize key genes related to pyroptosis. Initially, the "glmnet" R package was utilized for LASSO regression, where the optimal regularization parameter (λ) was determined through 10-fold cross-validation to select genes with non-zero coefficients. The stability of the LASSO-selected features was confirmed through 1000 iterations to mitigate overfitting. Simultaneously, an SVM model was established, and candidate genes were identified based on criteria such as high accuracy, low error rate, and minimal gene count.

For the screening of hypoxia-related key genes, we employed Random Forest (RF) and Generalized Linear Model (GLM). The dataset underwent a 7:3 partition into training and testing subsets, with model evaluation conducted through 5-fold cross-validation. Systematic assessment of model performance was carried out using the "DALEX" R package, which integrated two analytical approaches: ROC analysis for predictive accuracy quantification and residual distribution analysis for model consistency verification, ultimately determining the optimal model. The top 10 genes determined by the optimal model were selected and subsequently intersected with those identified through LASSO and SVM algorithms to pinpoint diagnostic genes.

Validation of Diagnostic Genes and RT-qPCR

A comparative group analysis was conducted on the validation dataset, GSE16561, to identify differential expression of diagnostic genes between the IS group and control groups. The association of these diagnostic genes with IS was systematically assessed by evaluating their diagnostic performance using ROC curves created with the "pROC" R package.[24] The area under the curve (AUC) metrics were calculated for both the training and external validation datasets to evaluate diagnostic performance.

Total RNA from peripheral blood was extracted using the RNA extraction kit provided by Servicebio. Subsequently, cDNA synthesis was performed in accordance with the manufacturer's guidelines using the TransScript cDNA synthesis kit. RT-qPCR was executed on the QuantStudio 5 platform employing the GenStar SYBR Green master mix. The specific sequences of the primers are outlined in Supplementary Table 3. The thermal cycling conditions were established as follows: an initial denaturation at 95°C for 2 minutes, followed by 40 cycles consisting of 95°C for 15 seconds and 60°C for 30 seconds, concluding with a melt curve analysis. The internal reference gene utilized in this analysis was GAPDH.

Immune Infiltration Analysis

To evaluate and contrast the heterogeneity of immune infiltration among 28 cell types in the IS and control cohorts, we utilized ssGSEA via the "GSVA" R package. This approach quantifies the proportional presence of individual immune cell infiltrates by annotating various categories of infiltrating immune cells and computing the enrichment score for each cell type. Additionally, we examined inter-subgroup heterogeneity within the immune microenvironment by comparing the pyroptosis- and hypoxia-related IS subgroups. Boxplots were employed to depict variations in immune cell abundance between groups, while lollipop charts were utilized to demonstrate significant relationships between diagnostic genes and immune cells.

GSEA of Diagnostic Genes

Diagnostic genes were profiled for regulatory pathways using single-gene GSEA methodology. IS Samples were stratified based on the median expression levels of the diagnostic genes. Reference gene sets ("c2.all.v2024.1.Hs.symbols.gmt") were sourced from the MSigDB. Functional enrichment analysis was conducted using the "clusterProfiler" R package, with Benjamini–Hochberg adjustment applied. Pathways with an adjusted p-value of < 0.05 were considered significantly enriched.

scRNA-Seq Data Processing

Two samples (GSM5319989 and GSM5319992) were chosen from the scRNA-seq dataset GSE174574 for analysis. Initially, raw data quality control was performed based on specific criteria: $200 < \text{nCount} < 5000$, $\text{nFeature} > 200$, complexity > 0.8, and mitochondrial gene proportions < 0.2. Subsequently, data normalization and standardization were carried out using the "Seurat" R package,[25] with identification and removal of doublets. Cell cycle processing was then executed, followed by PCA for dimensionality reduction. The top 20 principal components were selected for cell clustering with a resolution of 0.8 to delineate distinct cell populations. Post-clustering, data visualization was achieved through UMAP dimensionality reduction.[26] Cell population annotation was performed using the "MouseRNAseqData" as the reference file and the "SingleR" R package, which assigns the most similar reference cell type to each cell based on gene expression features, facilitating automatic cell-type annotation. Furthermore, expression levels of diagnostic genes across different cellular populations were computed, visualized using UMAP, and represented through violin plots and dot plots to illustrate variations in expression intensity among cell types. This analysis confirmed heightened expression of diagnostic genes in specific cellular subtypes.

Drug Prediction and Molecular Docking Analysis

In this study, we screened candidate drugs using the CMAP database (https://clue.io/query).[27] We merged and deduplicated previously identified pyroptosis-related DEGs and hypoxia-related DEGs before importing them into CMAP. The therapeutic potential of small-molecule compounds was evaluated via the normalized connectivity score (norm_cs), ranging from −3 to 3. Negative scores indicate a therapeutic effect by reversing disease-associated gene expression, with larger absolute values denoting stronger pharmacological activity.[28] To validate the CMAP-predicted candidates, we conducted protein-drug docking experiments with diagnostic genes. We obtained 3D structures of core target proteins from the UniProt database (https://www.uniprot.org/) and small molecules from the PubChem database (https://pubchem.ncbi.nlm.nih.gov/) in SDF format. Protein structures were preprocessed with PyMOL: removing water molecules and irrelevant ligands, retaining the single-chain protein encoded by the target gene, and saving in PDB format. Molecular docking was performed using the CB-DOCK2 platform (https://cadd.labshare.cn/cb-dock2/php/blinddock.php). The binding free energy, where more negative values indicate greater stability and binding affinity,[29] assessed protein-ligand interactions. By integrating CMAP-based drug prediction with molecular docking validation, we established an evaluation system for gene target-candidate drug interactions, supporting drug development for IS.

Statistical Analyses

All statistical analyses and visualizations for data mining were performed using R software (version 4.3.3; R Foundation for Statistical Computing, Vienna, Austria). Intergroup differences in gene expression were assessed using Wilcoxon rank-sum tests. The RT-qPCR experimental data, obtained from a minimum of three independent replicates, were analyzed with unpaired t-tests using GraphPad Prism 9.0. A p-value below 0.05 was deemed statistically significant, with the thresholds for significance established as follows: $^{*}p < 0.05$, $^{**}p < 0.01$, and $^{***}p < 0.001$.

Results

Identification of DEGs Associated with Pyroptosis and Hypoxia

The flowchart of this study is shown in Figure 1.

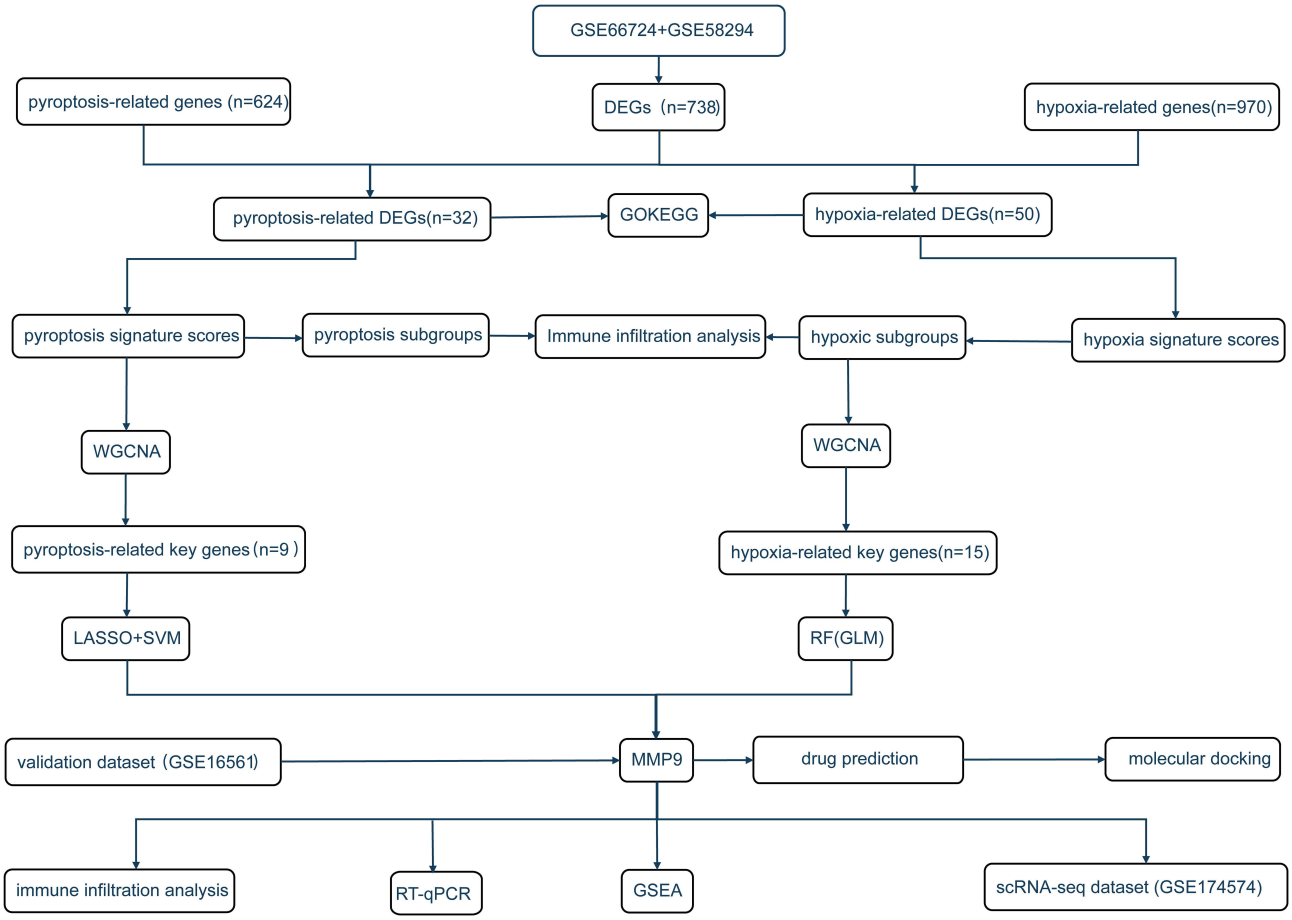

Figure 1 Flow chart of the study.

Expression profiles from the GSE66724 and GSE58294 datasets were merged into a training set. After addressing batch effects and normalizing using log2(x+1) transformation, the expression profiles across all samples showed high consistency. PCA plots were then constructed to depict sample distribution patterns pre- and post-batch effect correction (Figure 2A). Through differential expression analysis, 738 DEGs were recognized between the IS and control groups, with 337 upregulated and 401 downregulated genes (Figure 2B). Subsequent analysis of the intersection of DEGs with known pyroptosis-related genes and hypoxia-related genes unveiled 32 pyroptosis-related DEGs and 50 hypoxia-related DEGs. These findings were visually represented using Venn diagrams (Figure 2C and D) and heat maps (Figure 2E and F) to demonstrate gene set overlap and expression patterns, respectively.

GO/KEGG Analysis of Pyroptosis-Related DEGs and Hypoxia-Related DEGs

Systematic GO and KEGG enrichment analyses were performed to elucidate the signaling pathways and biological functions linked to the pyroptosis-related DEGs. The GO enrichment analysis results revealed that these genes were primarily associated with the positive regulation of cytokine production, regulation of the apoptotic signaling pathway, focal adhesion, cell-substrate junction, cadherin binding, DNA-binding transcription factor binding, and carbohydrate binding (Figure 3A). The KEGG enrichment analysis (Figure 3B) demonstrated significant involvement of these genes in Fluid shear stress and atherosclerosis, Lipid and atherosclerosis, and the tumor necrosis factor (TNF) signaling pathway.

To assess the functional landscape of the hypoxia-related DEGs, we conducted thorough functional enrichment analyses utilizing GO annotation and KEGG pathways. The GO annotation revealed significant enrichment in regulating apoptotic signaling pathways, promoting neurogenesis, enhancing phosphatidylinositol 3-kinase/protein kinase B signal transduction, as well as in membrane rafts, membrane microdomains, focal adhesion, dioxygenase activity, and

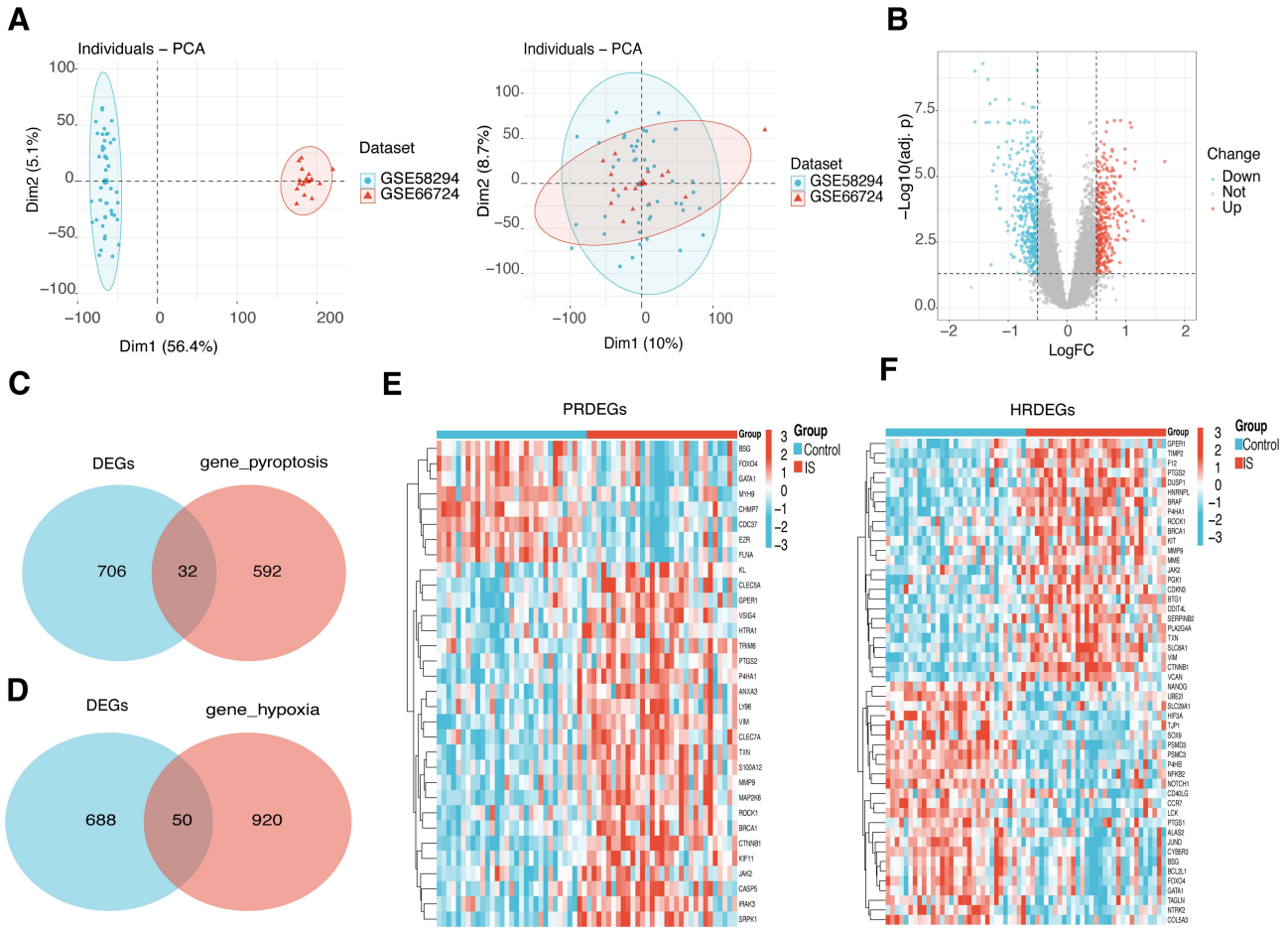

Figure 2 Identification of pyroptosis-related DEGs and hypoxia-related DEGs. (**A**) Merging of GSE66724 and GSE58294 datasets and batch effect removal; (**B**) Volcano plot of DEGs; (**C**) Venn diagram shows the cross genes between DEGs and pyroptosis-related genes; (**D**) Venn diagram shows the cross genes between DEGs and hypoxia-related genes; (**E**) Heat map of 32 pyroptosis-related DEGs; (**F**) Heat map of 50 hypoxia-related DEGs.

transcription coregulator binding (Figure 3C). Subsequent KEGG pathway analysis identified four key pathological modules: the MAPK signaling pathway, NF-κB signaling pathway, Fluid shear stress and atherosclerosis, and Arachidonic acid metabolism (Figure 3D).

Identification of Key Genes Associated with Pyroptosis Signature Scores and Hypoxic Subgroups Using WGCNA

In the investigation of using pyroptosis signature scores as clinical traits in IS samples, we applied WGCNA to systematically characterize gene modules closely associated with pyroptosis. The methodology involved several steps. Initially, we selected the top 25% of genes with the highest expression variance in the IS group and conducted hierarchical clustering of samples to eliminate outliers. Subsequently, we constructed a scale-free co-expression network with a soft-thresholding power of $\beta = 5$ (scale-free criterion: $R^2 = 0.9$) and identified core co-expression modules (Figure 4A). Utilizing hierarchical clustering in conjunction with a dynamic tree-cutting algorithm, we identified seven color-coded gene modules (minModuleSize = 100, mergeCutHeight = 0.5) (Figure 4B). Analysis of the relationship between modules and traits revealed a strong correlation between the yellow module (comprising 681 genes) and the pyroptosis signature scores ($|r| = 0.73$, $p = 2.58e\text{-}06$; Figure 4C). Finally, by intersecting genes within the yellow module with pyroptosis-related DEGs, we pinpointed nine key pyroptosis-related genes: VSIG4, MMP9, IRAK3, CASP5, ANXA3, SRPK1, ROCK1, JAK2 and MYH9 (Figure 4D).

https://doi.org/10.2147/IJGM.S550007

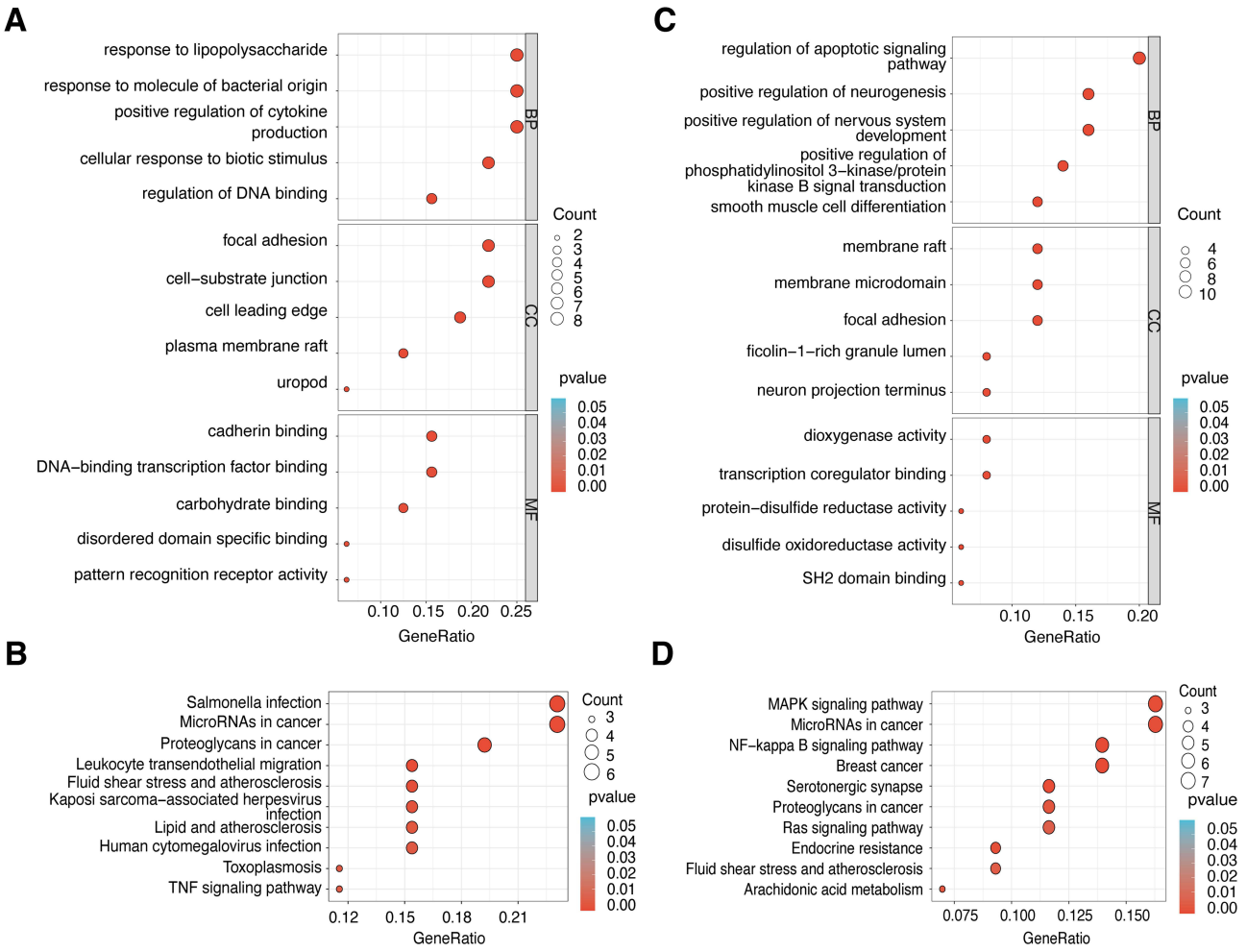

Figure 3 Functional enrichment analysis of pyroptosis-related DEGs and hypoxia-related DEGs. (**A** and **C**) The top five GO terms (BP, CC, and MF) represented by pyroptosis-related DEGs and hypoxia-related DEGs; (**B** and **D**) The top ten KEGG pathway analysis results of pyroptosis-related DEGs and hypoxia-related DEGs.

Furthermore, WGCNA was utilized to identify gene modules linked to hypoxic subgroups in IS samples. A scale-free co-expression network was constructed with a soft-thresholding power of $\beta = 5$ ($R^2 = 0.9$), leading to the identification of 11 distinct co-expression modules through hierarchical clustering and dynamic tree-cutting algorithms (Figure 4E). Module-trait analysis revealed significant associations between hypoxic subgroups and two modules: the yellow module ($|r| = 0.43$, $p = 0.0169$) and the blue module ($|r| = 0.45$, $p = 0.0116$) (Figure 4F). By integrating these modules with hypoxia-related DEGs, 15 key hypoxia-related genes (CTNNB1, SLC8A1, MMP9, TIMP2, KIT, ROCK1, JAK2, BRCA1, FOXO4, NOTCH1, ALAS2, BSG, CYB5R3, GATA1 and BCL2L1) were identified (Figure 4G).

Machine Learning Models Identify Diagnostic Genes for IS

The diagnostic utility of nine key genes associated with pyroptosis was evaluated in the training set using the LASSO regression algorithm (Figure 5A). Visualization analysis generated a coefficient trajectory plot (Figure 5B), elucidating the quantitative relationships between gene expression levels and log-transformed λ penalty coefficients. With decreasing penalty coefficient λ, the feature selection threshold became more stringent, ultimately identifying a set of five core genes: VSIG4, MMP9, IRAK3, JAK2, and MYH9. Subsequently, a feature selection model was established utilizing the SVM algorithm to maximize classification accuracy (Figure 5C) and achieve dual-criteria optimization while minimizing prediction errors (Figure 5D). The SVM model exhibited optimal discriminative performance by incorporating eight genes: MYH9, MMP9, CASP5, ANXA3, JAK2, VSIG4, IRAK3, and ROCK1.

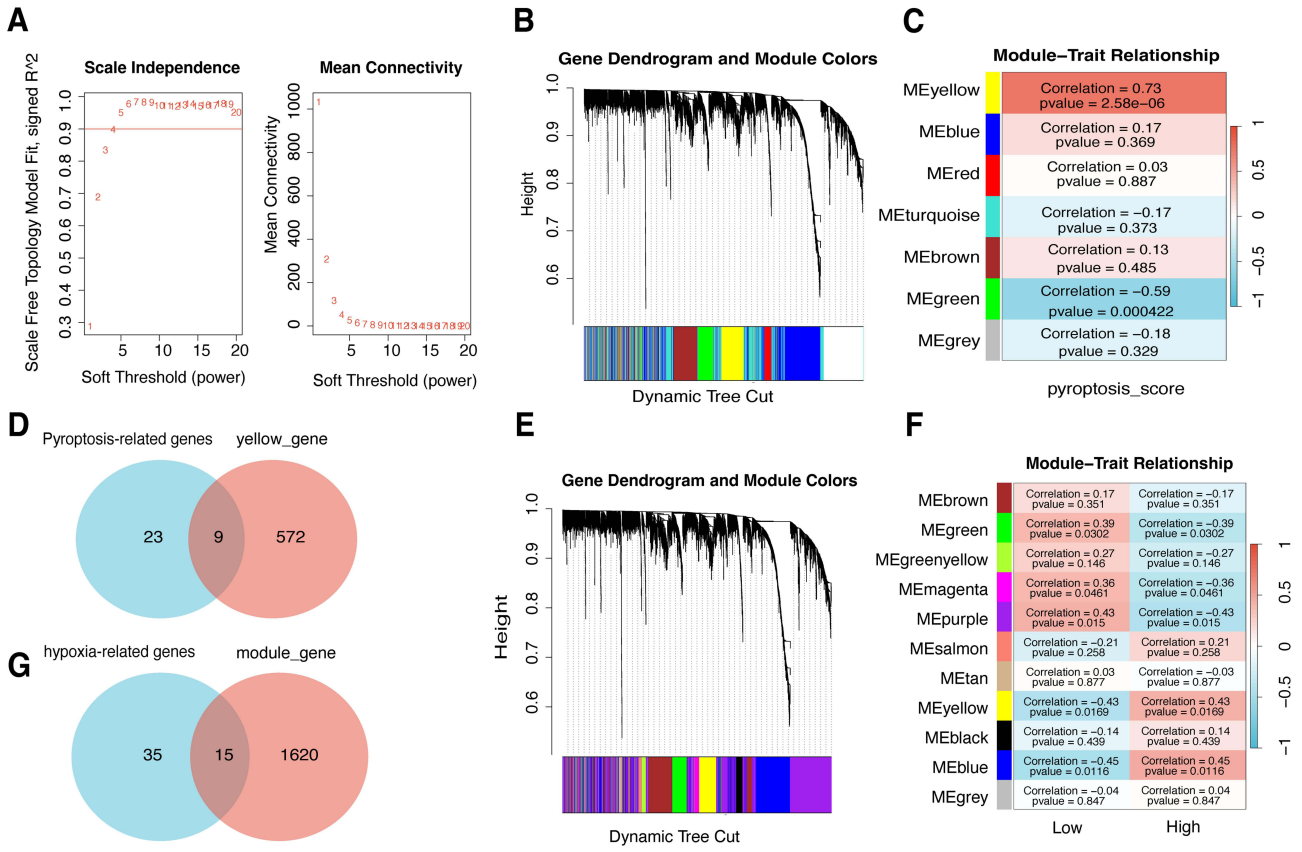

Figure 4 Identification of the key genes involved in pyroptosis signature scores and hypoxic subgroups in IS. (**A**) Analysis of the scale-free index and mean connectivity for various soft-thresholding powers; (**B**) Co-expressed genes of pyroptosis signature scores were analyzed using WGCNA; (**C**) The heatmap shows 7 gene modules in the different pyroptosis signature scores, correlations and p-values are contained in each module; (**D**) Venn diagram shows the cross genes between pyroptosis-related DEGs and module genes; (**E**) Co-expressed genes of hypoxic subgroups were analyzed using WGCNA; (**F**) The heatmap shows 11 gene modules in the different hypoxic subgroups; (**G**) Venn diagram shows the cross genes between hypoxia-related DEGs and module genes.

In the assessment of 15 hypoxia-related key genes, RF outperformed GLM, exhibiting more tightly clustered residual distributions (Figure 5E and F) and a significantly higher AUC of 0.914, indicating enhanced predictive accuracy in ROC analysis (Figure 5G). Consequently, RF was selected as the optimal model. Through feature importance assessment, the top 10 influential genes were identified as NOTCH1, TIMP2, SLC8A1, CYB5R3, CTNNB1, BRCA1, GATA1, BSG, MMP9, and BCL2L1. Figure 5H displays the top five genes ranked by the two algorithms.

By integrating the LASSO, SVM, and RF algorithms, MMP9 emerged as the sole gene common to all three methods via Venn analysis (Figure 5I), underscoring its significance as a critical diagnostic biomarker.

Validation of Diagnostic Gene

In the training set, the expression levels of MMP9 were significantly elevated in the IS group compared to the control group ($p < 0.001$) (Figure 6A). ROC analysis exhibited strong diagnostic accuracy, with an AUC of 0.794 (Figure 6B), indicating a robust discriminatory capacity for identifying IS. These results were consistently replicated in an independent cohort: Analysis of the GSE16561 dataset demonstrated significantly elevated MMP9 expression in patients with IS relative to controls ($p < 0.001$) (Figure 6C), resulting in an AUC of 0.853 (Figure 6D). Validation confirmed the significant differential expression of MMP9 between IS and control cohorts. The consistent diagnostic performance highlights the potential of MMP9 as a valuable biomarker for diagnosing IS.

Peripheral blood samples from healthy controls and patients with IS underwent RNA extraction and RT-qPCR analysis. Results revealed significantly elevated MMP9 expression in the IS group compared to controls ($p < 0.001$) (Figure 6E), aligning with bioinformatics analysis findings.

https://doi.org/10.2147/IJGM.S550007

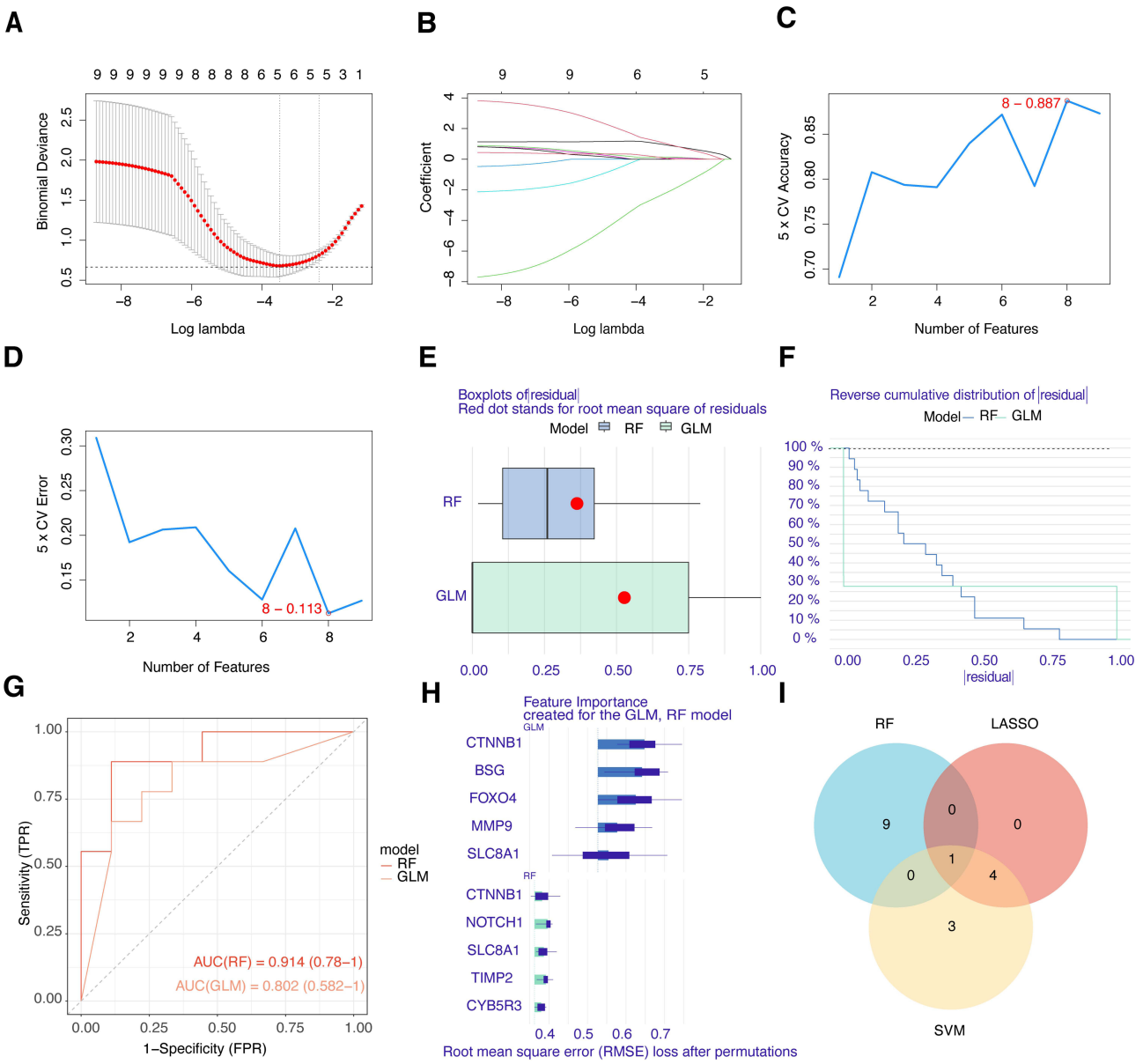

Figure 5 Identification of candidate diagnostic gene. (**A**) Selection of the optimal parameter for nonzero coefficients in the LASSO model; (**B**) Coefficient selection for the 5 hub genes based on LASSO analysis; (**C** and **D**) The error and accuracy analysis of SVM algorithm; (**E**) Boxplots of residuals in GLM and RF models, red dots indicating root mean square errors; (**F**) Reverse cumulative distribution of residuals in GLM and RF models; (**G**) The ROC curves predict the accuracy of each learning machine model; (**H**) Top five key genes in RF and GLM models; (**I**) The intersection of the three algorithms (MMP9).

Immune Infiltration Analysis

Analysis using ssGSEA identified significant alterations in the infiltration patterns of 28 immune cell subtypes between the IS and control groups, with 11 subtypes showing marked differences (Figure 7A). Specifically, central memory CD4+ T cells, eosinophils, immature dendritic cells, macrophages, memory B cells, and neutrophils exhibited heightened infiltration in IS patients, while activated B cells, effector memory CD4+/CD8+ T cells, immature B cells, and monocytes displayed decreased infiltration levels. Interestingly, the expression levels of MMP9 demonstrated a positive correlation with macrophages and neutrophils, whereas a negative correlation was observed with effector memory CD4+/CD8+ T cells (Figure 7B).

Stratified analyses further revealed distinct immune microenvironment profiles. The group with high pyroptosis scores exhibited increased infiltration of macrophages, myeloid-derived suppressor cells, memory B cells, neutrophils, and regulatory T cells, while showing decreased levels of effector memory CD8+ T cells and immature B cells

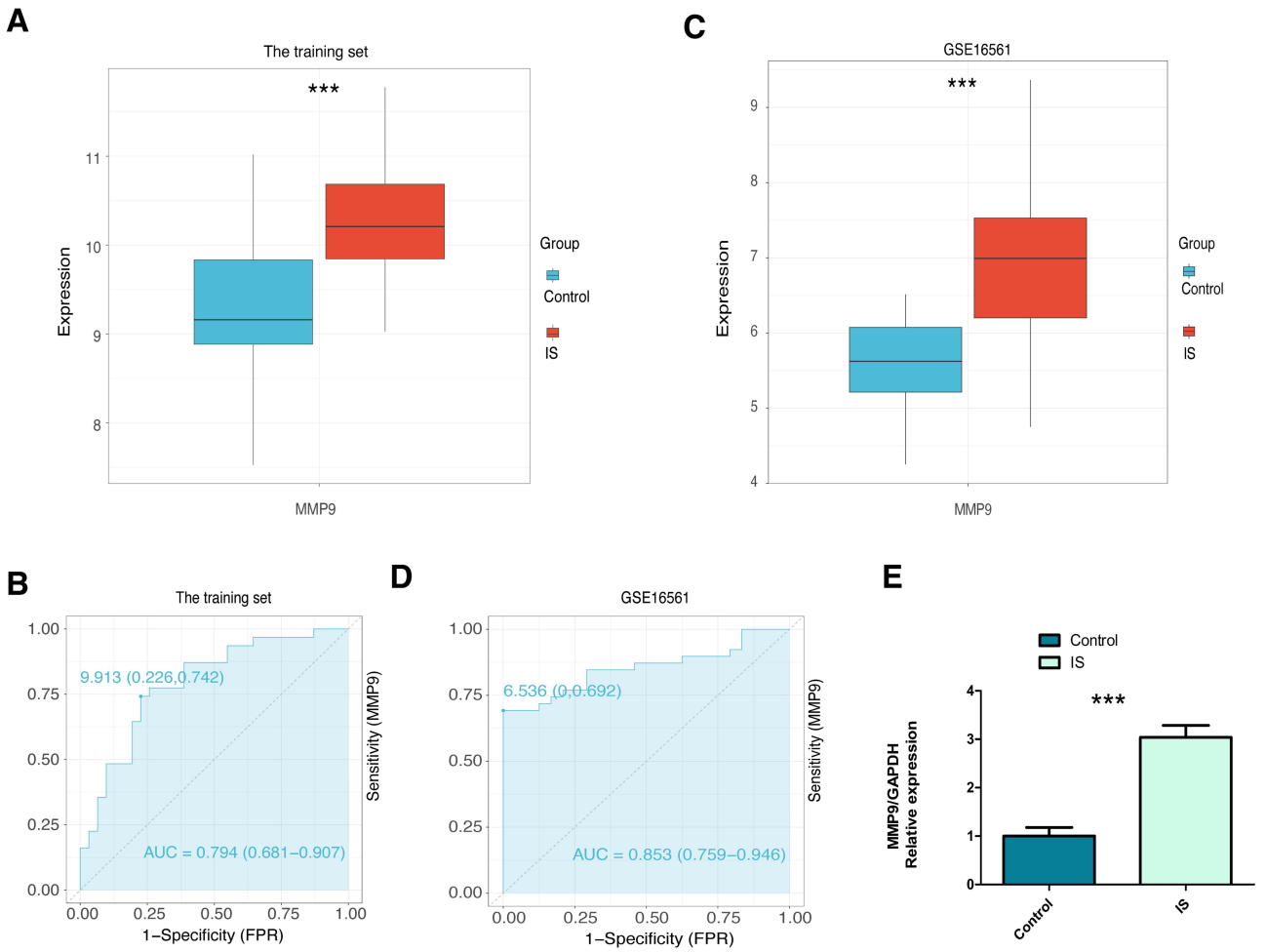

Figure 6 Verification of MMP9. (**A**) The expression of MMP9 in the training set; (**B**) The ROC curve of MMP9 in the training set; (**C**) The expression of MMP9 in GES16561 dataset; (**D**) The ROC curve of MMP9 in GES16561 dataset; (**E**) RT-qPCR validation, Comparison of gene expression between IS and control groups in MMP9. The symbol ns represents no statistical significance, $p < 0.05$ was considered statistically significant, indicated by *** for $p < 0.001$.

(Figure 7C). In the hypoxic subgroup, the high-scoring group displayed enrichment of activated dendritic cells, macrophages, neutrophils, and Th17 cells, alongside reduced abundance of activated CD4+/CD8+ T cells, central memory CD4+ T cells, effector memory CD8+ T cells, and Th2 cells (Figure 7D).

Macrophages and neutrophils exhibited consistent hyperinfiltration across all subgroups and maintained strong positive correlations with MMP9 expression ($p < 0.001$) (Figure 7E and F).

GSEA of MMP9

The function of diagnostic genes in IS was assessed through single-gene GSEA (Figure 7G). Our findings indicate a positive correlation between MMP9 and pathways related to hypoxia, NF-κB signaling, inflammatory response, immune system disorders, and neutrophil degranulation.

Single-Cell Level Expression of MMP9 in Mouse Brain

We employed clustering analysis to identify 21 distinct cell clusters (Figure 8A), which were subsequently annotated using the "SingleR" package and visualized on a UMAP plot (Figure 8B). Our analysis revealed nine discernible cell populations: astrocytes, endothelial cells, epithelial cells, fibroblasts, granulocytes, macrophages, microglia, monocytes, and oligodendrocytes. We then examined the expression of MMP9 across these cell populations on the UMAP plot of the

https://doi.org/10.2147/IJGM.S550007

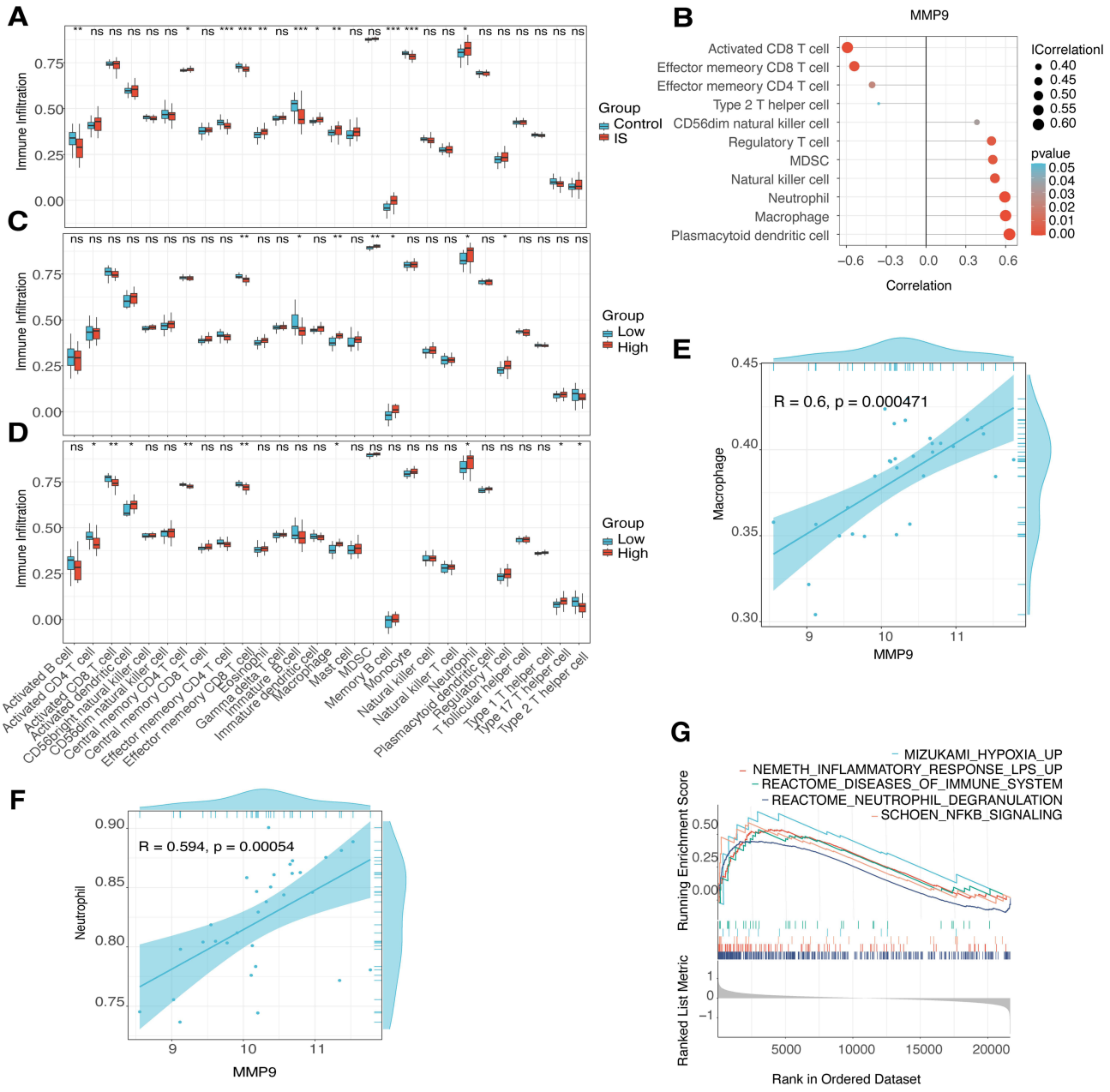

Figure 7 The ssGSEA analysis of immune cell infiltration and GSEA analysis of MMP9. (**A**) Box plot illustrating contrasting distribution patterns of immune cells between IS patients and control group; (**B**) Lollipop plot visualizing the correlation between MMP9 and immune cells; (**C**) Comparative analysis of immune cell distribution patterns across pyroptosis subgroups; (**D**) Comparative analysis of immune cell distribution patterns across hypoxia subgroups; (**E**) Scatter plot showing significant positive correlations between MMP9 expression and infiltration levels of macrophages; (**F**) Scatter plot showing significant positive correlations between MMP9 expression and infiltration levels of neutrophils; (**G**) The GSEA analysis of MMP9. The symbol ns represents no statistical significance, $p < 0.05$ was considered statistically significant, indicated by * for $p < 0.05$, ** for $p < 0.01$, and *** for $p < 0.001$.

IS group, allowing for the quantification of its expression levels (Figure 8C). Remarkably, granulocytes exhibited high levels of MMP9 expression (Figure 8D and E).

Drug Prediction and Molecular Docking for IS Therapy

The study identified 69 genes (Supplementary Table 4) by integrating and deduplicating 32 pyroptosis-related DEGs and 50 hypoxia-related DEGs. Drug prediction analysis using the CMAP database identified small-molecule compounds with therapeutic potential. Figure 9A lists the top five candidates with the highest positive and negative scores. Molecular docking simulations revealed that Benperidol and Fluspirilene, the two compounds with the lowest scores, form stable

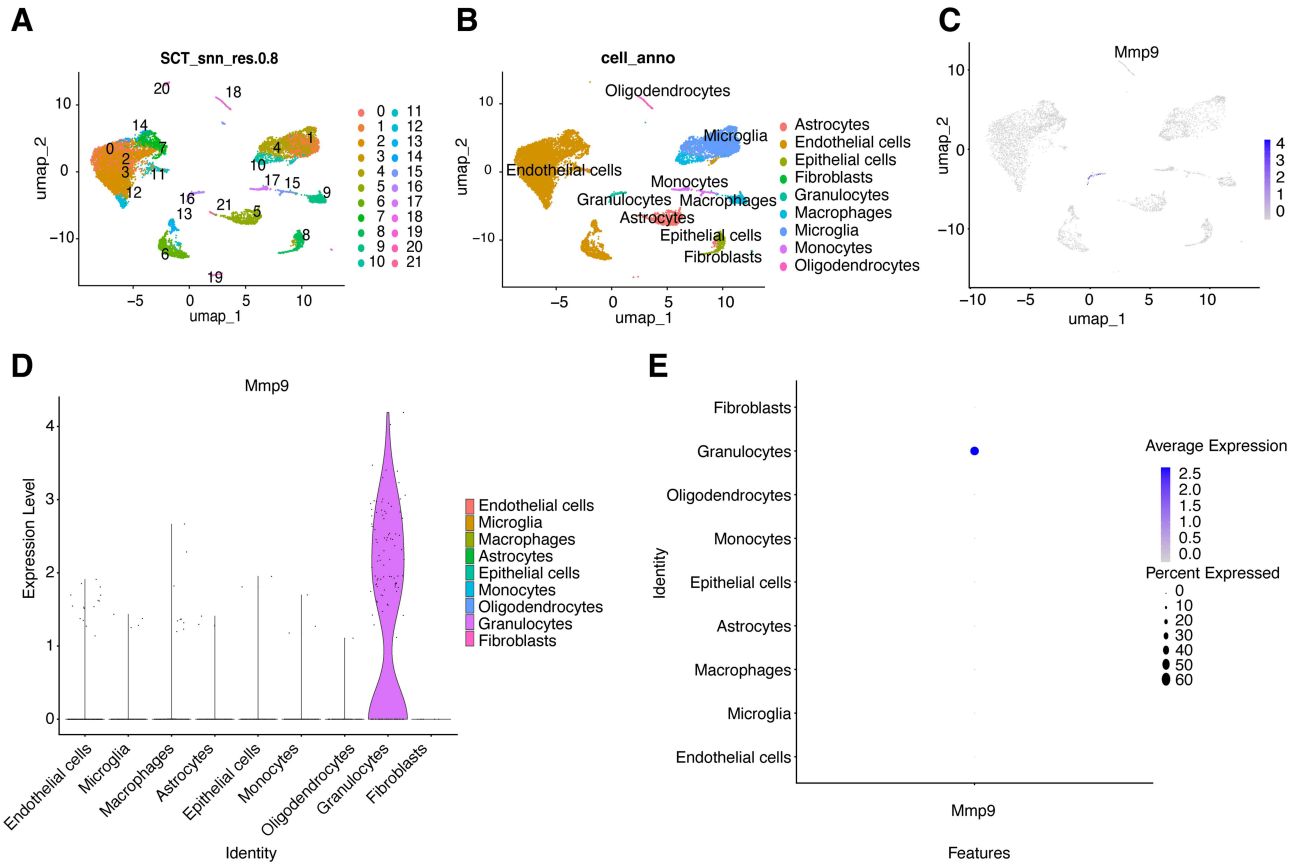

Figure 8 The scRNA-seq reveals the expression of Mmp9 in mouse brain. (**A**) 21 cell clusters classified based on scRNA-seq data; (**B**) The identification of 9 cell subtypes; (**C**) Distribution of Mmp9 across the various cell types in the GSE174574 dataset; (**D**) Violin plots illustrating Mmp9 distribution across distinct cell types; (**E**) Dot plots demonstrating Mmp9 distribution across distinct cell types.

binding conformations with MMP9, with binding energies of −9.6 kcal/mol and −10.3 kcal/mol, respectively. Figure 9B depicts the 2D structures of these compounds. Visualization via the CB-DOCK2 platform showed that Benperidol interacts with MMP9 through hydrogen bonds, hydrophobic interactions, and cation-π interactions, while Fluspirilene binds via hydrogen bonds, weak hydrogen bonds, hydrophobic interactions, cation-π interactions, and π-π stacking. These diverse interactions suggest MMP9 as a potential target for these compounds (Figure 9C and D).

Discussion

Ischemic stroke, a serious condition caused by inadequate cerebral blood flow due to thrombosis or vascular stenosis, results in neuronal damage. Growing evidence explores the interaction between pyroptosis and hypoxia in ischemic stroke,[30–32] offering fresh perspectives on disease progression. However, the therapeutic targets and underlying mechanisms are not yet fully understood. This study's comprehensive analysis of transcriptomic data from the GEO database identified DEGs linked to these two processes. Machine learning algorithms, such as LASSO, SVM, and RF, identified MMP9 as a key candidate gene. RT-qPCR analysis showed significantly increased MMP9 expression in the peripheral blood of patients with IS, with AUC values of 0.794 and 0.853 in the training and validation sets, respectively. These results confirm MMP9's diagnostic capability and highlight its potential clinical utility for IS diagnosis. Furthermore, our findings underscore the necessity of understanding the interplay between pyroptosis and hypoxia, as this may reveal new therapeutic targets and strategies for IS.

MMP9, a zinc-dependent endopeptidase, plays a crucial role in tissue remodeling and immune regulation by breaking down the extracellular matrix and modulating inflammatory factors.[33] During the early stages of IS, MMP9 expression significantly increases via the hypoxia-induced HIF-1α pathway, amplifying its influence on disease progression.

https://doi.org/10.2147/IJGM.S550007

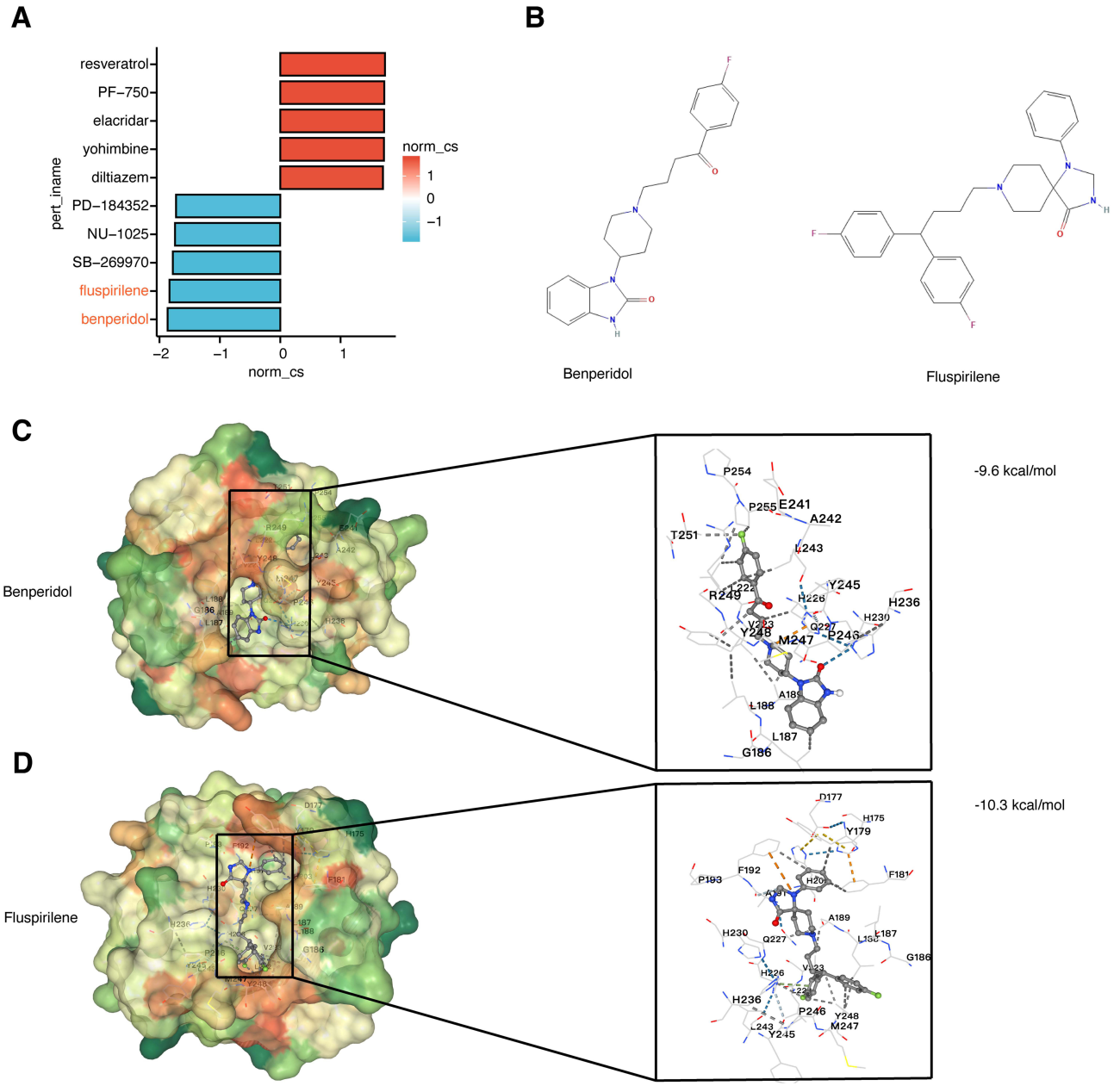

Figure 9 Drug prediction and molecular docking. (**A**) The top five small-molecule compounds with the highest positive and negative scores. The two compounds with the lowest scores, Benperidol and Fluspirilene, are highlighted in red; (**B**) The 2D structures of Benperidol and Fluspirilene; (**C** and **D**) Diagram of the binding mode of MMP9 with Benperidol and Fluspirilene.

Critically, active MMP9 undermines the structural integrity of the blood-brain barrier, leading to cerebral edema and the infiltration of inflammatory cells into the brain parenchyma, key events in early brain injury.[34] Beyond disrupting the blood-brain barrier, MMP9 also aggravates brain damage by amplifying inflammation. It activates pro-inflammatory cytokines (TNF-α, IL-1β) and releases chemokines from the extracellular matrix, creating a chemotactic gradient that attracts neutrophils and monocytes/macrophages to ischemic areas, thereby intensifying neuroinflammation and secondary tissue injury.[35] These findings highlight MMP9's critical role as a multifaceted mediator in cerebral ischemia pathogenesis, providing a basis for targeted therapeutic strategies.

Functional enrichment analysis of 32 pyroptosis-related DEGs and 50 hypoxia-related DEGs showed their predominant involvement in inflammatory responses and key pathways including NF-κB and TNF signaling. The coordinated activation of these pathways forms the central regulatory network driving neuroinflammation in IS.[36,37] At the molecular

level, NF-κB activation promotes microglial polarization toward the pro-inflammatory M1 phenotype and induces astrocyte conversion to neurotoxic A1 type. This process upregulates inflammatory mediators (TNF-α, IL-1β, ICAM-1), exacerbating blood-brain barrier disruption and neuronal programmed cell death.[38,39] TNF-α further establishes a positive feedback loop that sustains NF-κB activation, amplifying neurotoxic factor release (IL-6, IL-1β) and accelerating neuronal injury.[40] Mechanistically, MMP9 appears to amplify inflammasome-driven pyroptosis through TNF-α/NF-κB signaling axis activation, as evidenced by our GSEA revealing significant NF-κB pathway enrichment in MMP9-high IS samples.

The pathological progression of IS is profoundly influenced by the dynamic polarization and intercellular interactions of macrophages and neutrophils, which drive neuroinflammation and tissue damage.[41–43] N1-type neutrophils promote the polarization of M1-type macrophages by secreting neutrophil gelatinase-associated lipocalin, which subsequently releases pro-inflammatory factors such as TNF-α and IL-1β, amplifying the inflammatory cascade and exacerbating neuronal injury.[44] Our analysis of immune cell infiltration in IS patients revealed a significant positive correlation between the expression levels of MMP9 and the infiltration density of macrophages and neutrophils, particularly in subgroups with prominent pyroptosis features and populations exhibiting a hypoxic microenvironment. ScRNA-seq further demonstrated that MMP9 exhibits specific high expression in granulocytes within the ischemic penumbra region. These findings collectively elucidate the central regulatory role of MMP9 in stroke pathology. MMP9 not only serves as a key mediator in immune microenvironment remodeling but also drives the vicious cycle of post-stroke inflammatory storms by coordinating pyroptosis processes and hypoxic stress responses. In-depth understanding of the MMP9-mediated immune cell network regulatory mechanisms will provide critical insights into the pathological mechanisms of IS.

This study identified Benperidol and Fluspirilene as significantly linked to IS treatment through CMAP database screening. Molecular docking confirmed both compounds as high-affinity MMP9 ligands. This discovery not only enhances the understanding of MMP9's biological roles but also redefines it from a diagnostic marker to a therapeutic target with intervention potential. Fluspirilene, a dual inhibitor of sodium and calcium channels, exhibits modulation of multiple ion channels involved in neuronal excitability. Fluspirilene has been studied for central nervous system applications, indicating its ability to cross the blood-brain barrier, and to effectively penetrate target brain tissue. Following cerebral ischemia, Fluspirilene may exert neuroprotective effects by correcting neuronal calcium overload and sodium imbalance.[45,46] These results provide a novel theoretical foundation for multi-targeted therapeutic strategies in cerebrovascular diseases. While Benperidol exhibits strong MMP9 binding affinity, direct evidence of its efficacy in cerebral infarction is still absent, necessitating systematic preclinical studies to confirm its neuroprotective effects and mechanisms.

Our findings align with and extend previous investigations on MMP9's role in IS pathogenesis. The observed upregulation of MMP9 expression in the blood transcriptomes of patients with IS corroborates previous clinical reports documenting elevated serum MMP9 levels during the acute ischemic phases, reinforcing its potential as a diagnostic biomarker.[47] Preclinical evidence demonstrating that MMP9 inhibition ameliorates blood-brain barrier disruption and infarct volume in murine ischemia-reperfusion models further supports our findings,[48] suggesting the therapeutic potential of MMP9 modulation. Our bioinformatics analysis revealed for the first time that MMP9 serves as a critical mediator linking pyroptosis to hypoxia in the pathogenesis of IS. MMP9 appears to drive the polarization of M1-type macrophages via N1-type neutrophils, leading to the release of pro-inflammatory factors such as TNF-α. This process amplifies the inflammatory cascade through activation of the TNF-α/NF-κB signaling axis, thereby exacerbating neuronal injury.

Despite employing rigorous methodologies, this study has notable limitations. Firstly, data were exclusively sourced from peripheral blood samples in public databases, lacking validation in brain tissues or disease-specific cell populations. The small clinical cohort may also limit the biomarkers' generalizability. Secondly, the molecular mechanism by which MMP9 influences the immune microenvironment via pyroptosis-hypoxia synergy remains unvalidated through gene editing or functional experiments. Moreover, the single-cell sequencing analysis was restricted to granulocyte subset expression profiles, overlooking other microenvironment components. Lastly, while candidate drugs predicted by CMAP have been validated by molecular docking, their blood-brain barrier penetration and therapeutic efficacy still require assessment both in vitro and in vivo. Although Benperidol demonstrated high binding affinity in molecular docking, direct evidence of its efficacy in IS is still lacking. In subsequent studies, we will integrate ADMET predictions with in vivo animal model experiments to further evaluate the clinical applicability of the candidate drugs.

Conclusions

This study identifies MMP9 as a pivotal pyroptosis-hypoxia synergistic effector in IS, showing strong diagnostic potential through multi-cohort validation and RT-qPCR. Its upregulation leads to immune dysregulation via macrophage/neutrophil infiltration. Drug screening suggests Benperidol and Fluspirilene as high-affinity therapeutic candidates. This study further confirms and systematically validates the diagnostic value and potential therapeutic implications of MMP9 in IS.

Abbreviations

IS, Ischemic stroke; DEGs, Differentially expressed genes; WGCNA, Weighted gene co-expression network analysis; RT-qPCR, real-time quantitative PCR; LASSO, Least Absolute Shrinkage and Selection Operator; SVM, Support Vector Machine; RF, Random Forest; scRNA-seq, Single-cell RNA sequencing; MMP9, Matrix metalloproteinase-9; MCAO, Middle cerebral artery occlusion; PCA, Principal component analysis; GO, Gene Ontology; KEGG, Kyoto Encyclopedia of Genes and Genomes; GSEA, Gene set enrichment analysis; GLM, Generalized Linear Model; ROC, Receiver Operating Characteristic; AUC, Area under the curve.

Data Sharing Statement

The datasets GSE66724, GSE58294, and GSE17457 were obtained from the GEO database (https://www.ncbi.nlm.nih.gov/geo/); the phenotype-related genes associated with pyroptosis and hypoxia were sourced from the GeneCard (https://www.genecards.org) and MSigDB (https://www.gsea-msigdb.org/gsea/msigdb/index.jsp) databases.

Ethics Approval and Consent to Participate

This study was approved by the Ethics Committee of Yixing People's Hospital (Approval No.: Lun Shen 2025 Ke 038-01). Participant recruitment occurred from March to September, 2025, and written informed consent was acquired from the family members of all participating patients.

Consent for Publication

All authors have given consent for publication.

Acknowledgments

The authors would like to thank the GEO databases for providing data for the study and those authors who uploaded valuable.

Author Contributions

All authors made a significant contribution to the work reported, whether that is in the conception, study design, execution, acquisition of data, analysis and interpretation, or in all these areas; took part in drafting, revising or critically reviewing the article; gave final approval of the version to be published; have agreed on the journal to which the article has been submitted; and agree to be accountable for all aspects of the work.

Funding

This work was supported by grants from the Key Project of the 2023 Medical-Education Collaborative Innovation Fund of Jiangsu University (grant number JDY2023011) and the Youth Research Project of the Wuxi Health Commission (grant number Q201940).

Disclosure

The authors report no conflicts of interest in this work.

References

1. GBD 2019 Stroke Collaborators. Global, regional, and national burden of stroke and its risk factors, 1990–2019: a systematic analysis for the Global Burden of Disease Study 2019. *Lancet Neurol*. 2021;20(10):795–820. doi:10.1016/S1474-4422(21)00252-0

2. Campbell BCV, Majoie CBLM, Albers GW, et al; HERMES collaborators. Penumbral imaging and functional outcome in patients with anterior circulation ischaemic stroke treated with endovascular thrombectomy versus medical therapy: a meta-analysis of individual patient-level data. *Lancet Neurol*. 2019;18(1):46–55. doi:10.1016/S1474-4422(18)30314-4
3. Alrafiah A, Alofi E, Almohaya Y, et al. Angiogenesis biomarkers in ischemic stroke patients. *J Inflamm Res*. 2021;14:4893–4900. doi:10.2147/JIR.S331868
4. Rodríguez-Yáñez M, Castillo J. Role of inflammatory markers in brain ischemia. *Curr Opin Neurol*. 2008;21(3):353–357. doi:10.1097/WCO.0b013e3282ffafbf
5. Nong J, Glassman PM, Shuvaev VV, et al. Targeting lipid nanoparticles to the blood-brain barrier to ameliorate acute ischemic stroke. *Mol Ther*. 2024;32(5):1344–1358. doi:10.1016/j.ymthe.2024.03.004
6. Xia J, Zhang Y, Zhao H, et al. Non-invasive monitoring of CNS MHC-I molecules in ischemic stroke mice. *Theranostics*. 2017;7(11):2837–2848. doi:10.7150/thno.18968
7. Weng WT, Kuo PC, Scofield BA, et al. 4-ethylguaiacol modulates neuroinflammation and promotes heme oxygenase-1 expression to ameliorate brain injury in ischemic stroke. *Front Immunol*. 2022;13:887000. doi:10.3389/fimmu.2022.887000
8. Valančienė J, Melaika K, Šliachtenko A, et al. Stroke genetics and how it informs novel drug discovery. *Expert Opin Drug Discov*. 2024;19(5):553–564. doi:10.1080/17460441.2024.2324916
9. Gou X, Xu D, Li F, et al. Pyroptosis in stroke: new insights into disease mechanisms and therapeutic strategies. *J Physiol Biochem*. 2021;77(4):511–529. doi:10.1007/s13105-021-00817-w
10. Li L, Shi C, Dong F, et al. Targeting pyroptosis to treat ischemic stroke: from molecular pathways to treatment strategy. *Int Immunopharmacol*. 2024;133:112168. doi:10.1016/j.intimp.2024.112168
11. Ye A, Li W, Zhou L, et al. Targeting pyroptosis to regulate ischemic stroke injury: molecular mechanisms and preclinical evidences. *Brain Res Bull*. 2020;165:146–160. doi:10.1016/j.brainresbull.2020.10.009
12. Wang Y, Guan X, Gao CL, et al. Medioresinol as a novel PGC-1α activator prevents pyroptosis of endothelial cells in ischemic stroke through PPARα-GOT1 axis. *Pharmacol Res*. 2021;169:105640. doi:10.1016/j.phrs.2021.105640
13. Yan H, Huang W, Rao J, Yan D, Yuan J. Demethylase FTO-mediated m6A modification of lncRNA MEG3 activates neuronal pyroptosis via NLRP3 signaling in cerebral ischemic stroke. *Mol Neurobiol*. 2024;61(2):1023–1043. doi:10.1007/s12035-023-03622-2
14. Du O, Yan YL, Yang HY, et al. ALPK1 signaling pathway activation by HMGB1 drives microglial pyroptosis and ferroptosis and brain injury after acute ischemic stroke. *Int Immunopharmacol*. 2025;149:114229. doi:10.1016/j.intimp.2025.114229
15. Huang Y, Xu W, Zhou R. NLRP3 inflammasome activation and cell death. *Cell Mol Immunol*. 2021;18(9):2114–2127. doi:10.1038/s41423-021-00740-6
16. Stelzer G, Rosen N, Plaschkes I, et al. The GeneCards suite: from gene data mining to disease genome sequence analyses. *Curr Protoc Bioinformatics*. 2016;54:1.30.1–1.30.33. doi:10.1002/cpbi.5
17. Liberzon A, Birger C, Thorvaldsdóttir H, et al. The Molecular Signatures Database (MSigDB) hallmark gene set collection. *Cell Syst*. 2015;1(6):417–425. doi:10.1016/j.cels.2015.12.004
18. Bakka AG, Patil SS, Rachakonda B, et al. Breaking barriers in stroke therapy: recent advances and ongoing challenges. *Cureus*. 2025;17(1):e78288. doi:10.7759/cureus.78288
19. Leek JT, Johnson WE, Parker HS, Jaffe AE, Storey JD. The SVA package for removing batch effects and other unwanted variation in high-throughput experiments. *Bioinformatics*. 2012;28(6):882–883. doi:10.1093/bioinformatics/bts034
20. Ritchie ME, Phipson B, Wu D, et al. Limma powers differential expression analyses for RNA-sequencing and microarray studies. *Nucleic Acids Res*. 2015;43(7):e47. doi:10.1093/nar/gkv007
21. Wu T, Hu E, Xu S, et al. ClusterProfiler 4.0: a universal enrichment tool for interpreting omics data. *Innovation*. 2021;2(3):100141. doi:10.1016/j.xinn.2021.100141
22. Hänzelmann S, Castelo R, Guinney J. GSVA: gene set variation analysis for microarray and RNA-Seq data. *BMC Bioinf*. 2013;14:7. doi:10.1186/1471-2105-14-7
23. Langfelder P, Horvath S. WGCNA: an R package for weighted correlation network analysis. *BMC Bioinf*. 2008;9:559. doi:10.1186/1471-2105-9-559
24. Robin X, Turck N, Hainard A, et al. pROC: an open-source package for R and S+ to analyze and compare ROC curves. *BMC Bioinf*. 2011;12:77. doi:10.1186/1471-2105-12-77
25. Butler A, Hoffman P, Smibert P, Papalexi E, Satija R. Integrating single-cell transcriptomic data across different conditions, technologies, and species. *Nat Biotechnol*. 2018;36(5):411–420. doi:10.1038/nbt.4096
26. Becht E, McInnes L, Healy J, et al. Dimensionality reduction for visualizing single-cell data using UMAP. *Nat Biotechnol*. 2018;36:1213–1222.
27. Huang Y, Yue S, Qiao J, et al. Identification of diagnostic genes and drug prediction in metabolic syndrome-associated rheumatoid arthritis by integrated bioinformatics analysis, machine learning, and molecular docking. *Front Immunol*. 2024;15:1431452. doi:10.3389/fimmu.2024.1431452
28. Karube K, Tsuzuki S, Yoshida N, et al. Comprehensive gene expression profiles of NK cell neoplasms identify vorinostat as an effective drug candidate. *Cancer Lett*. 2013;333(1):47–55. doi:10.1016/j.canlet.2012.12.022
29. Zhou H, Fu H, Shao X, et al. Identification of novel inhibitors for epidermal growth factor receptor tyrosine kinase using absolute binding free-energy simulations. *Int J Biol Macromol*. 2025;304(Pt 2):140989. doi:10.1016/j.ijbiomac.2025.140989
30. Wang Z, Duan Y, Wu Y, et al. Research progress on the pyroptosis mediated by the NLRP3 inflammasome in the pathology of ischemic stroke. *Xi Bao Yu Fen Zi Mian Yi Xue Za Zhi*. 2024;40(7):648–654.
31. Yao M, Wang X, Lin H, et al. LncRNA Tug1 regulates post-stroke microglial pyroptosis via PINK1/Parkin-mediated mitophagy. *Inflammation*. 2024;48:2677–2691. doi:10.1007/s10753-024-02219-8
32. Zhuang H, Lei W, Wu Q, et al. Overexpressed CD73 attenuates GSDMD-mediated astrocyte pyroptosis induced by cerebral ischemia-reperfusion injury through the A2B/NF-κB pathway. *Exp Neurol*. 2025;386:115152. doi:10.1016/j.expneurol.2025.115152
33. Liu M, Zhang H, Li Y, et al. Loss of MMP9 disturbs cranial suture fusion via suppressing cell proliferation, chondrogenesis and osteogenesis in mice. *Matrix Biol*. 2024;134:93–106. doi:10.1016/j.matbio.2024.10.003
34. Shackleton B, Ringland C, Abdullah L, et al. Influence of matrix metallopeptidase 9 on beta-amyloid elimination across the blood-brain barrier. *Mol Neurobiol*. 2019;56(12):8296–8305. doi:10.1007/s12035-019-01672-z
35. Buttacavoli M, Di Cara G, Roz E, et al. Integrated multi-omics investigations of metalloproteinases in colon cancer: focus on MMP2 and MMP9. *Int J Mol Sci*. 2021;22(22):12389. doi:10.3390/ijms222212389

36. Lv H, Li J, Che YQ. CXCL8 gene silencing promotes neuroglial cells activation while inhibiting neuroinflammation through the PI3K/Akt/NF-κB-signaling pathway in mice with ischemic stroke. *J Cell Physiol*. 2019;234(5):7341–7355. doi:10.1002/jcp.27493
37. Qian J, Guo X, Xu Q, Huang Z. Therapeutic potential of TPT-260 in ischemic stroke: an investigation into its anti-inflammatory effects and impact on microglial activation. *J Inflamm Res*. 2025;18:3055–3066. doi:10.2147/JIR.S497030
38. Wang S, Pan Y, Zhang C, et al. Transcriptome analysis reveals dynamic microglial-induced A1 astrocyte reactivity via C3/C3aR/NF-κB signaling after ischemic stroke. *Mol Neurobiol*. 2024;61(12):10246–10270. doi:10.1007/s12035-024-04210-8
39. Yan W, Wang C, Zhao Y, Jiang Y, Sun M. Involvement of calpain in neurovascular unit damage through up-regulating PARP-NF-κB signaling during experimental ischemic stroke. *Mol Neurobiol*. 2024;61(10):8104–8122. doi:10.1007/s12035-024-04092-w
40. Wang P, Li C, Liao G, et al. Vanillin attenuates proinflammatory factors in a tMCAO mouse model via inhibition of TLR4/NF-κB signaling pathway. *Neuroscience*. 2022;491:65–74. doi:10.1016/j.neuroscience.2022.03.003
41. Jian Z, Liu R, Zhu X, et al. The involvement and therapy target of immune cells after ischemic stroke. *Front Immunol*. 2019;10:2167. doi:10.3389/fimmu.2019.02167
42. Beuker C, Strecker JK, Rawal R, et al. Immune cell infiltration into the brain after ischemic stroke in humans compared to mice and rats: a systematic review and meta-analysis. *Transl Stroke Res*. 2021;12(6):976–990. doi:10.1007/s12975-021-00887-4
43. Liu Q, Sorooshyari SK. Quantitative and correlational analysis of brain and spleen immune cellular responses following cerebral ischemia. *Front Immunol*. 2021;12:617032. doi:10.3389/fimmu.2021.617032
44. Hou Y, Yang D, Zhang Q, et al. Pseudoginsenoside-F11 ameliorates ischemic neuron injury by regulating the polarization of neutrophils and macrophages in vitro. *Int Immunopharmacol*. 2020;85:106564. doi:10.1016/j.intimp.2020.106564
45. Spedding M, Kenny B, Chatelain P. New drug binding sites in Ca2+ channels. *Trends Pharmacol Sci*. 1995;16(4):139–142. doi:10.1016/S0165-6147(00)89002-1
46. Shaw V, Srivastava S, Srivastava SK. Repurposing antipsychotics of the diphenylbutylpiperidine class for cancer therapy. *Semin Cancer Biol*. 2021;68:75–83. doi:10.1016/j.semcancer.2019.10.007
47. Wendt TS, Gonzales RJ. Ozanimod differentially preserves human cerebrovascular endothelial barrier proteins and attenuates matrix metalloproteinase-9 activity following in vitro acute ischemic injury. *Am J Physiol Cell Physiol*. 2023;325(4):C951–C971. doi:10.1152/ajpcell.00342.2023
48. Amruta N, Bix G. ATN-161 ameliorates ischemia/reperfusion-induced oxidative stress, fibro-inflammation, mitochondrial damage, and apoptosis-mediated tight junction disruption in Bend.3 cells. *Inflammation*. 2021;44(6):2377–2394. doi:10.1007/s10753-021-01509-9